AMERICAN SOCIETY FOR MICROBIOLOGY | Applied and Environmental Microbiology®

PHYSIOLOGY

Insights into the Function of the *N*-Acetyltransferase SatA That Detoxifies Streptothricin in *Bacillus subtilis* and *Bacillus anthracis*

Rachel M. Burckhardt,[a] Jorge C. Escalante-Semerena[a]

[a]Department of Microbiology, University of Georgia, Athens, Georgia, USA

ABSTRACT Acylation of epsilon amino groups of lysyl side chains is a widespread modification of proteins and small molecules in cells of all three domains of life. Recently, we showed that *Bacillus subtilis* and *Bacillus anthracis* encode the GCN5-related *N*-acetyltransferase (GNAT) SatA that can acetylate and inactivate streptothricin, which is a broad-spectrum antibiotic produced by actinomycetes in the soil. To determine functionally relevant residues of *B. subtilis* SatA (*Bs*SatA), a mutational screen was performed, highlighting the importance of a conserved area near the C terminus. Upon inspection of the crystal structure of the *B. anthracis* Ames SatA (*Ba*SatA; PDB entry 3PP9), this area appears to form a pocket with multiple conserved aromatic residues; we hypothesized this region contains the streptothricin-binding site. Chemical and site-directed mutagenesis was used to introduce missense mutations into *satA*, and the functionality of the variants was assessed using a heterologous host (*Salmonella enterica*). Results of isothermal titration calorimetry experiments showed that residue Y164 of *Ba*SatA was important for binding streptothricin. Results of size exclusion chromatography analyses showed that residue D160 was important for dimerization. Together, these data advance our understanding of how SatA interacts with streptothricin.

IMPORTANCE This work provides insights into how an abundant antibiotic found in soil is bound to the enzyme that inactivates it. This work identifies residues for the binding of the antibiotic and probes the contributions of substituting side chains for those in the native protein, providing information regarding hydrophobicity, size, and flexibility of the antibiotic binding site.

KEYWORDS *Bacillus anthracis*, *Bacillus subtilis*, *N*-acetyltransferases, streptothricin, antibiotic resistance

Microbial antibiotic resistance is a challenging medical problem in the United States and throughout the world. According to data from the Centers for Disease Control and Prevention (CDC), 23,000 people die annually because of antibiotic-resistant infections (1). Microorganisms are a reservoir for antibiotic resistance genes, allowing them to adapt and live in diverse environments. For example, soil organisms must survive in the presence of diverse plant- and microbe-derived antimicrobial chemicals (2, 3). Streptothricin is the most common antibiotic produced by bacteria in the soil, and it consists of three parts: a streptolidine, a gulosamine moiety, and a β-lysine chain that varies from 1 to 7 units (Fig. 1) (4). Streptothricins cause mRNA mistranslation and protein synthesis inhibition by interacting with the ribosome (5, 6) and, thus, exert toxicity against Gram-positive and Gram-negative bacteria and fungi (7). Streptothricins are highly toxic and are not used clinically (8) but have been approved as a fungicide in China (9).

Several streptomycete species synthesize streptothricin. These bacteria encode an

Citation Burckhardt RM, Escalante-Semerena JC. 2019. Insights into the function of the *N*-acetyltransferase SatA that detoxifies streptothricin in *Bacillus subtilis* and *Bacillus anthracis*. Appl Environ Microbiol 85:e03029-18. https://doi.org/10.1128/AEM.03029-18.

Editor Marie A. Elliot, McMaster University

Address correspondence to Jorge C. Escalante-Semerena, jcescala@uga.edu.

Received 17 December 2018
Accepted 9 January 2019
Accepted manuscript posted online 18 January 2019
Published 6 March 2019

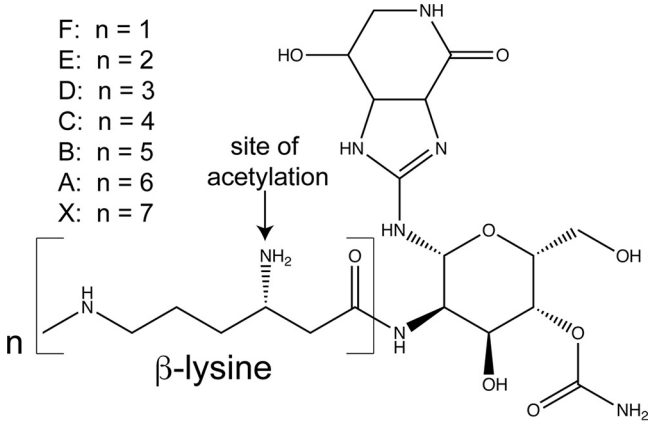

FIG 1 Structure of streptothricin. Streptothricins are comprised of a streptolidine, a gulosamine moiety, and a β-lysine chain that varies from one to seven units. This figure is a modification of a figure published in reference 26.

acetyltransferase to protect themselves from the antibiotic, as has been shown in *Streptomyces lavendulae* (10), *Streptomyces noursei* (11, 12), and *Streptomyces rochei* (13). Chemical modification is a common survival mechanism for bacteria to avoid the negative effects of antibiotics. Notable examples of this form of antibiotic resistance are chloramphenicol and kanamycin resistance; both antibiotics can be inactivated by acetyltransferases (14–18). A broadly distributed family of acetyltransferase enzymes belong to the GCN5-related *N*-acetyltransferase (GNAT) protein superfamily (PF00583), of which the yeast histone acetyltransferase GCN5 (19) is the founding member.

GNATs share limited sequence homology but do have a common core domain consisting of six or seven β-strands and four α-helices (19). The pyrophosphate binding loop between β4 and α3 allows for hydrogen bonding with acetyl coenzyme A (AcCoA). Another characteristic feature of GNATs is the "β-bulge" on the β4 strand, which splays beta strands β4 and β5 to create a V shape that allows for hydrogen bonding of the pantothenate arm of AcCoA (20).

While the binding of AcCoA is well established, how GNATs recognize and bind their ligand is less understood. Although some work has been done to explore how acetyltransferases interact with aminoglycoside ligands (21–25), an in-depth look at the chemical and steric implications of specific residues in a putative streptothricin-binding pocket is lacking. We recently characterized the streptothricin acetyltransferase SatA from *Bacillus subtilis*, and the crystal structure of the SatA from *Bacillus anthracis* has been determined (PDB entry 3PP9). Since the SatA proteins of these bacteria are 34% identical (54% similar), we decided to use the crystal structure of the *B. anthracis* protein to probe for residues important for function and how this GNAT may bind streptothricin.

RESULTS

Little is known about the mechanism of catalysis of the *N*-acetyltransferase responsible for the detoxification of streptothricin (Fig. 1) by either *Bacillus anthracis* or *Bacillus subtilis*. To gain insights into the function of this enzyme, we performed site-directed and unbiased mutagenesis to isolate proteins with different levels of functionality. Changes exerted by different side chains at a specific location were analyzed, with emphasis on the binding of streptothricin to the variants. The functionality of the variants was assessed using *Salmonella enterica*, an enterobacterium that is naturally susceptible to streptothricin (26) and provides a genetically tractable model system for understanding what is necessary and sufficient for streptothricin resistance.

Substitution at position L128 or A137 abolishes *B. subtilis* SatA (*Bs*SatA) activity *in vivo*. We used chemical mutagenesis to introduce missense mutations into plasmid-carried *B. subtilis satA*$^+$. A lysate of the high-transducing bacteriophage P22

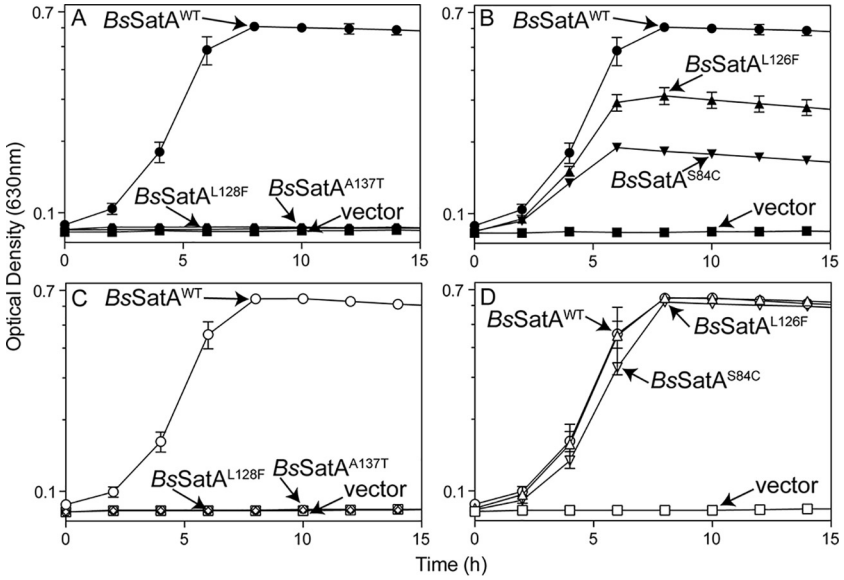

FIG 2 Variant *B. subtilis satA* alleles cannot confer streptothricin resistance in *S. enterica*. Strains carrying the wild type (*B. subtilis satA*$^+$, circles), variant *B. subtilis satA* alleles, or empty vector (squares) were grown in glycerol (22 mM) minimal medium and challenged with 10 μM streptothricin either without inducer (closed symbols) (A and B) or with 200 μM L-(+)-arabinose (open symbols) (C and D). Names next to arrows represent the protein produced by each strain. The following strains were analyzed: JE22263 (Δ*metE2702 ara-9*/pCV1; squares), JE22334 (Δ*metE*2702 *ara-9*/pBsSATA1; circles), JE23884 (Δ*metE2702 ara-9*/pBsSATA10; diamonds), JE23887 (Δ*metE2702 ara-9*/pBsSATA11; triangles), JE23888 (Δ*metE2702 ara-9*/pBsSATA12; hexagons), and JE23889 (Δ*metE2702 ara-9*/pBsSATA13; downward triangles). Error bars represent one standard deviation. vector, pCV1 (27).

carrying the plasmid with the *B. subtilis satA*$^+$ allele was treated with hydroxylamine, and the resulting plasmids were transduced into *S. enterica* strain JE7088 (*ara-9* Δ*metE*), screening for resistance to streptothricin (10 μM). Streptothricin-sensitive strains were further analyzed.

Four *B. subtilis satA* alleles encoded single-amino-acid variants that had substantially reduced or abolished activity (Fig. 2A and B). These alleles were cloned into an arabinose-inducible vector used for complementation studies in *S. enterica* (27, 28). All tested strains grew to full density when streptothricin was absent (see Fig. S1 in the supplemental material). *S. enterica* strains synthesizing the *Bs*SatA^{L128F} or *Bs*SatA^{A137T} variant were sensitive to streptothricin (10 μM) (Fig. 2A). These results suggested that the residues L128 and A137 play a role in protein folding, oligomerization, substrate binding, or catalysis. In previous studies, we showed that *S. enterica* strains that synthesize *Bs*SatA^{WT} are resistant to 10 μM streptothricin without the addition of inducer (26), indicating that the P_{BAD} promoter of pCV1 allows for enough residual expression of *satA* in the absence of arabinose to confer resistance. Importantly, adding arabinose to the medium (200 μM) did not overcome the inhibitory effect of streptothricin when the tester strain synthesized either the *Bs*SatA^{L128F} or *Bs*SatA^{A137T} variant (Fig. 2C), suggesting that the variants had little to no residual activity.

In contrast, *S. enterica* strains that synthesized *Bs*SatA^{L126F} or *Bs*SatA^{S84C} variants protected the cell against 10 μM streptothricin, albeit to a lesser degree than a strain that synthesized *Bs*SatA^{WT} (Fig. 2B). Addition of arabinose (200 μM) to the medium stimulated growth of the strains synthesizing *Bs*SatA^{L126F} and *Bs*SatA^{S84C}, matching the growth rate and culture density reached when the strain expressed *Bs*SatA^{WT} (Fig. 2D).

***Bs*SatA variants acetylate streptothricin *in vitro*.** To explore the effect of the above-mentioned substitutions on *Bs*SatA function, the enzymatic activity of the variants was quantified *in vitro* using a continuous spectrophotometric assay. For this purpose, *satA* alleles encoding the above-mentioned *Bs*SatA variants were cloned into an overproduction vector (27). We purified the wild type and variants of *Bs*SatA with a

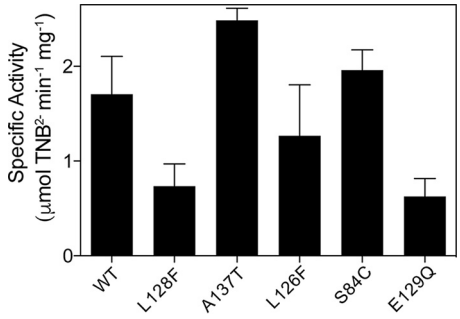

FIG 3 Specific activity of *Bs*SatA and variants. Reaction mixtures of acetyl-CoA, streptothricin, and H_6-*Bs*SatA and variants were incubated at 25°C, and specific activity was measured using a continuous spectrophotometric assay as described in Materials and Methods.

hexahistidine tag fused at its N terminus (H_6-*Bs*SatA) as described in Materials and Methods. We determined that H_6-*Bs*SatA^{WT} was active; hence the tag was not removed.

In vitro activity assays were performed with *Bs*SatA^{WT} and variant *Bs*SatA proteins. As shown in Fig. 3, all variants retained some level of activity. The *Bs*SatA^{L128F} variant had only ~40% of the activity of the wild-type enzyme, a result that was consistent with our observation that this variant could not detoxify streptothricin in *S. enterica* in the absence of inducer (Fig. 2A). Surprisingly, the specific activity of the *Bs*SatA^{A137T} variant was greater than that of *Bs*SatA^{WT} (Fig. 3), even though this variant also could not support growth of *S. enterica* strains challenged with streptothricin in the absence of induction (Fig. 2A). The *Bs*SatA^{L126F} or *Bs*SatA^{S84C} variants had activity levels similar to that of the wild type. Thus, all of the H_6-*Bs*SatA variants did acetylate streptothricin *in vitro* to various degrees.

The oligomeric state of all the purified *Bs*SatA variants was determined by size exclusion chromatography using fast protein liquid chromatography (FPLC). Previously, we showed that *Bs*SatA^{WT} forms dimers in solution (26). The retention time of all *B. subtilis Bs*SatA variants was consistent with a dimeric state (Table 1), suggesting that the impaired ability to confer streptothricin resistance in *S. enterica* by the *Bs*SatA variants was not due to a block in dimerization.

***Bs*SatAs variants with altered streptothricin affinity.** The binding affinity for streptothricin was measured for all *Bs*SatA variants in an effort to establish a correlation between reduced affinity and impaired streptothricin detoxification activity. As shown in Table 2, all variants bound streptothricin, albeit with different affinities. The dissociation constant (K_d) of streptothricin for the *Bs*SatA^{S84C} variant was almost 2-fold higher than that of *Bs*SatA^{WT}, which might account for the impaired, but not abolished, activity *in vivo* (Fig. 2B). In contrast, the affinity of the *Bs*SatA^{L126F} variant for streptothricin was similar to that for *Bs*SatA^{WT}; surprisingly, *Bs*SatA^{L126F} did not protect the cell as efficiently as *Bs*SatA^{WT} against streptothricin (Fig. 2B) unless the gene encoding it was overexpressed (Fig. 2D). For the *Bs*SatA^{L128F} and *Bs*SatA^{A137T} variants, which could not detoxify streptothricin *in vivo*, their affinities for streptothricin were lower by >4-fold (Table 2 and Fig. 4A versus B). This decrease in affinity for the substrate could explain the sensitivity to streptothricin of cells that synthesized either one of these variants (Fig. 2A), even when the genes encoding them were overexpressed (Fig. 2C).

Residue E129 may be an active-site base in *Bs*SatA. Surprisingly, none of the alleles found in our mutagenesis screen seemed to indicate an active-site base. Previous studies have shown a glutamate triggering a nucleophilic attack on the carbonyl of AcCoA (20, 29). To explore the possibility of elucidating the active-site base of *Bs*SatA, we examined the protein sequence alignment of known streptothricin acetyltransferases and noted that residues E93 and E129 of *Bs*SatA were conserved (Fig. 5). We inserted glutamine in each of these locations to remove the hydroxyl group while still retaining similar side chain length. Strains synthesizing variants *Bs*SatA^{E93Q} and *Bs*SatA^{E129Q} were challenged with 10 μM streptothricin as previously performed. Cells

TABLE 1 Size exclusion chromatography behavior of *B. subtilis* and *B. anthracis* SatA variants[a]

Variant	Molecular mass (kDa)	Oligomeric state (*n*)
Bacillus subtilis SatA		
*Bs*SatA monomer (predicted)	23	1
*Bs*SatA^{WT}	37	1.7
*Bs*SatA^{S84C}	39	1.7
*Bs*SatA^{L126F}	40	1.7
*Bs*SatA^{L128F}	33	1.4
*Bs*SatA^{A137T}	47	2
Bacillus anthracis SatA		
*Ba*SatA monomer (predicted)	24.5	1
*Ba*SatA^{WT}	50	2
*Ba*SatA^{Y149G}	56	2.3
*Ba*SatA^{Y149A}	55	2.2
*Ba*SatA^{Y149S}	55.5	2.3
*Ba*SatA^{Y149L}	49	2
*Ba*SatA^{Y149F}	59	2.4
*Ba*SatA^{Y149W}	55	2.2
*Ba*SatA^{F154G}	50	2
*Ba*SatA^{F154L}	56	2.3
*Ba*SatA^{F154Y}	50	2
*Ba*SatA^{F154W}	49	2
*Ba*SatA^{D160G}	168	Aggregate
*Ba*SatA^{D160A}	174	Aggregate
*Ba*SatA^{D160E}	467	Aggregate
*Ba*SatA^{D160N}	316	Aggregate
*Ba*SatA^{Y164G}	45	1.8
*Ba*SatA^{Y164A}	48	2
*Ba*SatA^{Y164S}	58	2
*Ba*SatA^{Y164L}	48.5	2
*Ba*SatA^{Y164F}	50	2
*Ba*SatA^{Y164W}	49	2

[a]Calculated molecular masses and oligomeric states for H_6-*Bs*SatA, H_6-*Ba*SatA, and their variants are shown. Samples were applied to a Superose 12 10/300 size exclusion column, and retention data were compared to a calibration curve generated from standards to calculate molecular mass.

synthesizing the *Bs*SatA^{E93Q} variant grew in the presence of streptothricin, although not as well as the strain carrying the wild-type *satA* allele (Fig. 6). In contrast, cells synthesizing the *Bs*SatA^{E129Q} variant did not grow in the presence of streptothricin, even with the addition of inducer (Fig. 6). Surprisingly, the purified *Bs*SatA^{E129Q} variant still retained *in vitro* activity under saturating conditions, although the activity was significantly reduced (~40% reduction, $P < 0.0001$). These data suggested that residue E129 is the active-site base.

***Bs*SatA^{WT} shows higher affinity for streptothricin than *Ba*SatA^{WT}.** Previously, we showed that the SatA homologue of *Bacillus anthracis* also has streptothricin acetyltransferase activity (26). However, using *S. enterica* as a tester strain, *B. anthracis* SatA (*Ba*SatA) conferred streptothricin resistance only upon induction of expression of the *B. anthracis satA*$^+$ gene (26). In light of these results, we sought to determine why *Bs*SatA was more effective than *Ba*SatA at streptothricin detoxification *in vivo*.

A possible explanation for the observed differences was provided by results of quantitative substrate affinity measurements. From such experiments we learned that the K_d for streptothricin for *Ba*SatA^{WT} was ~4-fold higher than that of *Bs*SatA^{WT} (Table 2 and Fig. 4A versus C). This is in line with the fact that the apparent K_m for streptothricin of *Ba*SatA^{WT} was ~3-fold higher than that for *Bs*SatA^{WT} (Table 3). This decrease in affinity for the streptothricin substrate would be consistent with the need for larger amounts of the *Ba*SatA protein to provide resistance to streptothricin in *S. enterica*.

Identification of aromatic residues that are important to *Ba*SatA function. As mentioned above, the crystal structure of *Ba*SatA is known (PDB entry 3PP9). The protein crystallized as a dimer, a result that was consistent with our size exclusion

TABLE 2 Streptothricin binding affinities of *B. subtilis* and *B. anthracis* SatA variants

Variant	K_d[a] (μM)
*Bs*SatA^{WT}	1.0
*Bs*SatA^{S84C}	1.7
*Bs*SatA^{L126F}	0.9
*Bs*SatA^{L128F}	4.3
*Bs*SatA^{A137T}	4.3
*Ba*SatA^{WT}	3.7
*Ba*SatA^{Y149G}	4.5
*Ba*SatA^{Y149A}	1.6
*Ba*SatA^{Y149S}	1.0
*Ba*SatA^{Y149L}	2.0
*Ba*SatA^{Y149F}	4.6
*Ba*SatA^{Y149W}	6.3
*Ba*SatA^{F154G}	1.0
*Ba*SatA^{F154L}	ND
*Ba*SatA^{F154Y}	0.5
*Ba*SatA^{F154W}	ND
*Ba*SatA^{D160G}	NB
*Ba*SatA^{D160A}	NB
*Ba*SatA^{D160E}	NB
*Ba*SatA^{D160N}	NB
*Ba*SatA^{Y164G}	NB
*Ba*SatA^{Y164A}	NB
*Ba*SatA^{Y164S}	NB
*Ba*SatA^{Y164L}	8.7
*Ba*SatA^{Y164F}	10.4
*Ba*SatA^{Y164W}	96

[a]ND, not determined; NB, not binding. Values represent the averages from three measurements.

chromatography data (Table 1). Upon examination of the crystal structure, we noticed that three conserved aromatic residues (Y149, F154, and Y164; all highlighted in blue in Fig. 5) appeared to form a cleft near the AcCoA binding site (Fig. S3). Random mutagenesis of the *B. subtilis satA* gene introduced substitutions L128F and A137T in this same area (Fig. 5, asterisks under red highlight) that led to variants with decreased affinity for streptothricin (Table 2), suggesting that this area is part of the structure where SatA binds streptothricin. Recently, Stogios et al. showed that the antibiotic tobramycin binds to 6′-*N*-acetyltransferase [AAC(6′)-Ib] in an open cleft (30), highlighting the possibility that streptothricin binds to this region of SatA.

We introduced substitutions at positions Y149, F154, and Y164 using the *B. anthracis satA*$^+$ allele by site-directed mutagenesis. Various substitutions were made for each of these three conserved aromatic residues to determine the chemical and steric impact of each side chain. Alanine and glycine substitutions were used to assess the overall impact of the size and chemistry of the replaced residue, with glycine allowing freer rotation of the amino acid backbone. We wished to explore the effects that the aliphatic side chain of leucine or the bulkier indole side chain of tryptophan would have on enzyme function when these side chains were introduced in lieu of phenylalanine or tyrosine. We also explored the effect of the absence of the hydroxyl moiety of tyrosine by substituting phenylalanine for tyrosine at positions Y149 and Y164.

The mutant alleles were cloned into arabinose-inducible vectors routinely used in complementation studies and tested *in vivo* in our *S. enterica* heterologous system to assess streptothricin resistance. All strains grew in minimal medium (Fig. S2) in the absence of streptothricin, but strains synthesizing the *Ba*SatA variants showed decreased streptothricin detoxification *in vivo* and were susceptible to streptothricin at much lower concentrations than the strain synthesizing *Ba*SatA^{WT} (Table 4). We decided to explore the growth kinetics of these strains at two streptothricin concentrations (5 μM or 10 μM) to understand how the substituted residue impacted detoxification. We also assessed whether adding more inducer could rescue the cells synthesizing these variants. Previous studies showed that *Ba*SatA conferred streptothricin resistance in *S. enterica* only upon induction of expression of the *B. anthracis satA*$^+$ gene (26).

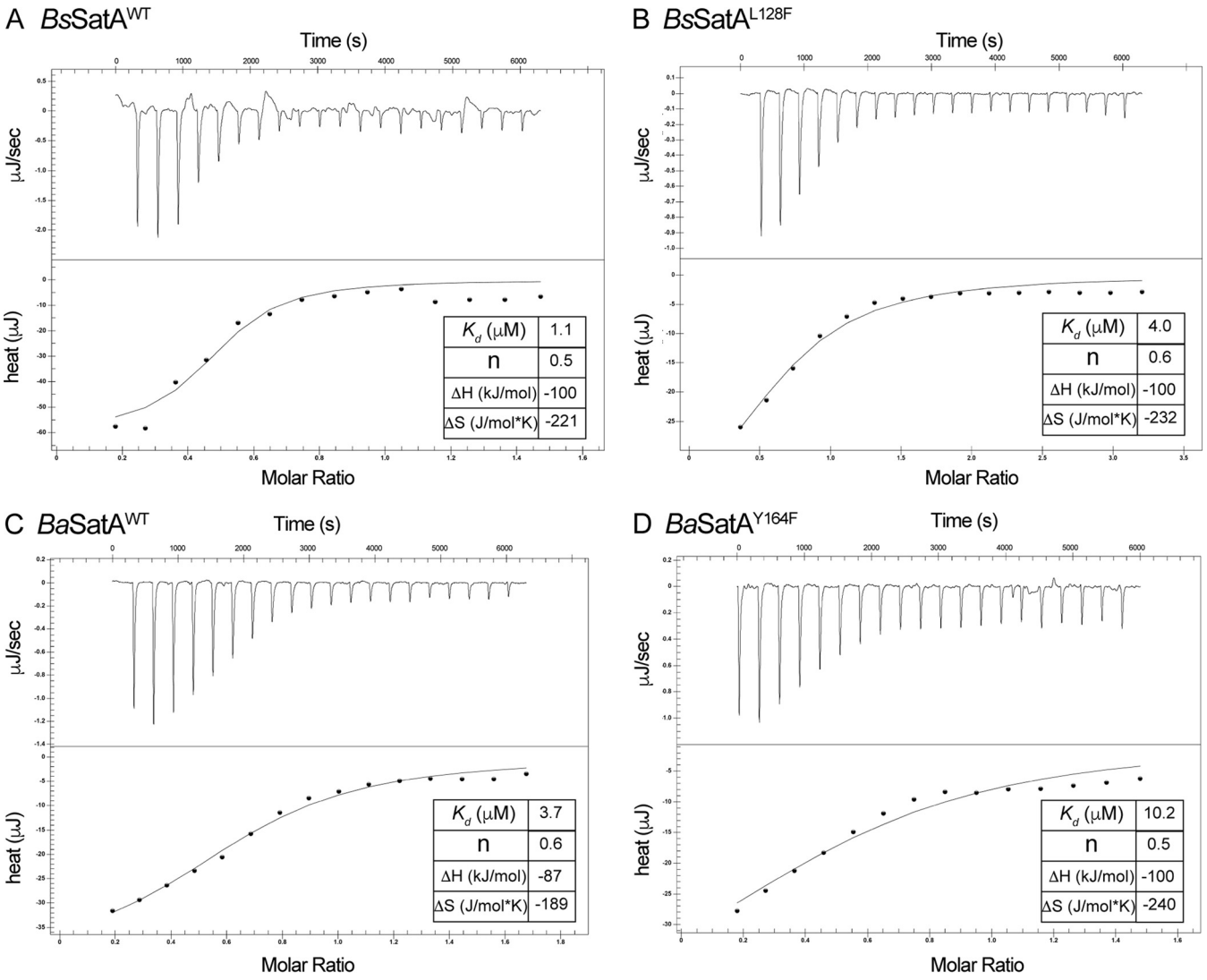

FIG 4 Representative streptothricin affinity determination experiments. Conditions for the performance of ITC experiments are detailed in Materials and Methods. (A and C) Isotherms of streptothricin binding to *Bs*SatA^{WT} and *Ba*SatA^{WT}, respectively. (B and D) Isotherms of streptothricin binding to *Bs*SatA^{L128F} and *Ba*SatA^{Y164F}. In all cases the insets show the thermodynamic parameters of the binding events. Each experiment was performed thrice, and the dissociation constants shown in the insets are for a single experiment. They differ slightly from those shown in Table 2, because those shown in Table 2 are averages from the three experimental values. Data for panel A were previously published (26) and are being used as a point of reference.

Thus, all strains carrying *B. anthracis satA* alleles were grown in medium containing 250 μM arabinose. In some cases, we increased the concentration of arabinose to 0.5 mM to determine the effect of increased detoxifying activity in the strains.

When strains were challenged with 5 μM (Fig. 7, columns E and F) or 10 μM (Fig. 7, columns G and H) streptothricin, only the strain that synthesized *Ba*SatA^{WT} (open circles) grew without delay. All of the *Ba*SatA variants conferred decreased streptothricin detoxification *in vivo* (Fig. 7), with the F154 substitutions having the least severe impact (Fig. 7, row B). Clearly, substitutions of these three conserved aromatic residues negatively impacted the ability of *Ba*SatA to detoxify streptothricin.

***In vitro* assessment of *Ba*SatA variants with substitutions at positions Y149, F154, and Y164.** To determine the impact of each substituted side chain on the enzymatic activity of *Ba*SatA, mutant alleles were cloned into overproduction vectors, and N-terminal hexahistidine *Ba*SatA variants were purified as described in Materials and Methods. Specific activities were quantified using a continuous spectrophotometric assay. As shown in Fig. 8, all *Ba*SatA variants displayed reduced activity, consistent

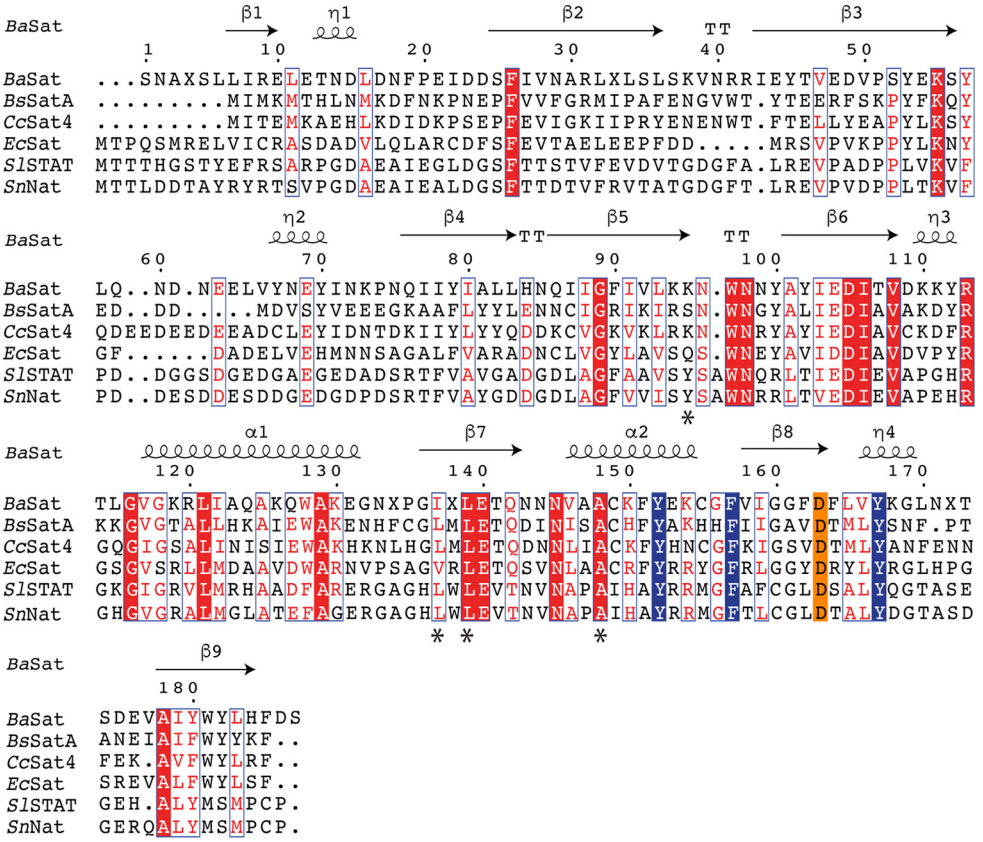

FIG 5 Alignment of various streptothricin acetyltransferase proteins. Streptothricin acetyltransferase protein sequences were aligned using Geneious software (https://www.geneious.com), and the figure was generated using ESPript. Conserved residues are highlighted red, while similar residues are boxed. Structural components of the *Bacillus anthracis* SatA homologue are shown above the indicated protein sequence; β refers to a β strand, TT refers to a turn, η refers to a 3_{10} helix, and α refers to an α helix. Numbers refer to the residue number of the crystalized *B. anthracis* SatA, which has three amino acids added at the N terminus. Residues substituted in the *B. subtilis* SatA (S84, L126, L128, and A137) are indicated with asterisks below the residue. Conserved residues of a putative streptothricin binding pocket are highlighted. Three conserved aromatic residues (blue) and an aspartic acid (orange) were substituted in the *B. anthracis* SatA.

with the *in vivo* studies (Fig. 7). However, these data did not explain why the substitutions led to less active variants.

To determine whether the various substitutions impacted the binding for streptothricin, the *Ba*SatA variants were tested using isothermal titration calorimetry (ITC) to

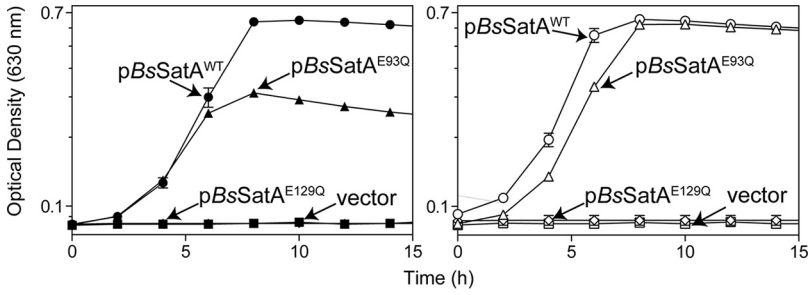

FIG 6 *B. subtilis* SatA^{E129Q} cannot confer streptothricin resistance in *S. enterica*. Strains carrying wild-type alleles (*B. subtilis satA*$^+$, circles), variant *B. subtilis satA* alleles, or empty vector (squares) were grown in glycerol (22 mM) minimal medium, challenged with 10 μM streptothricin either without inducer (closed symbols) or with 250 μM L-(+)-arabinose (open symbols). The following strains were analyzed: JE22263 (Δ*metE2702 ara-9*/pCV1; squares), JE22334 (Δ*metE*2702 *ara-9*/pBsSATA1; circles), JE24032 (Δ*metE2702 ara-9*/pBsSATA9; diamonds), and JE23657 (Δ*metE2702 ara-9*/pBsSATA4; triangles). Error bars represent one standard deviation. vector, pCV1 (27).

TABLE 3 Kinetic and binding parameters of *Ba*SatA[a]

Compound	$K_{m\ (app)}$ (μM)	K_{cat} (s^{-1})	K_{cat}/K_m ($M^{-1}\ s^{-1}$)	K_d (μM)
Streptothricin	2.8 ± 0.4	2.5×10^3	8.9×10^8	3.7
Acetyl-CoA	32 ± 7	3.3×10^3	1.0×10^8	ND

[a]Kinetic parameters were obtained from technical triplicates in two separate experiments. ND, not determined.

determine the thermodynamic parameters of streptothricin binding (Table 2). Surprisingly, some variants with substitutions of residue Y149 had affinities for streptothricin similar to those of the wild-type enzyme, even though these variants showed substantially reduced specific activity (Fig. 8). These data suggested that the reduced activity of the Y149 variants was due to a change other than altered streptothricin binding.

Changes at residue F154 led to the least severe impact of streptothricin detoxification in *S. enterica* (Fig. 7, row B), consistent with the fact that these variants retained more *in vitro* activity than the variants with the other substituted residues (Fig. 8). However, the impact of substitutions at F154 had substantial negative effects on streptothricin binding (Table 2). Binding affinities for the *Ba*SatA^{F154L} and *Ba*SatA^{F154W} variants were not obtained, because the proteins were unstable during the course of the ITC experiment.

Substitutions to the Y164 residue led to variants with a much lower affinity for streptothricin (Table 2 and Fig. 4C versus D), suggesting that Y164 plays a role in streptothricin binding. The *Ba*SatA^{Y164G} and *Ba*SatA^{Y164A} variants were unable to bind streptothricin (Table 2), while the K_d for the *Ba*SatA^{Y164F} variant increased by ~3-fold. This difference in substrate affinity indicated the importance of the hydroxyl group of tyrosine for streptothricin binding. We also substituted Ser at positions Y164 or Y149 to determine the impact of the bulkiness of the side chain while retaining the hydroxyl group. Notably, the *Ba*SatA^{Y164S} variant could not bind streptothricin (Table 2), suggesting that the phenyl group of Y164 was required for streptothricin binding.

A conserved aspartic acid is necessary for dimerization of *Ba*SatA. In the putative streptothricin-binding pocket of *Ba*SatA there is the conserved aspartic acid residue, D160 (Fig. 5, orange). Various substitutions were made at this location, including D160G, D160A, D160E, and D160N. The goal was to increase rotation with glycine, eliminate the negative charge with alanine, extend the side chain by one methylene with glutamate, or eliminate the negative charge with asparagine. The effect of the

TABLE 4 Streptothricin MICs of *S. enterica* strains carrying *B. anthracis satA* alleles[a]

Variant	MIC (μM)
*Ba*SatA^{WT}	60
Vector	1
*Ba*SatA^{Y149G}	1.5
*Ba*SatA^{Y149A}	2
*Ba*SatA^{Y149L}	1
*Ba*SatA^{Y149F}	2
*Ba*SatA^{Y149W}	11
*Ba*SatA^{F154A}	11
*Ba*SatA^{F154G}	11
*Ba*SatA^{F154L}	20
*Ba*SatA^{F154Y}	8
*Ba*SatA^{F154W}	4
*Ba*SatA^{D160G}	2
*Ba*SatA^{D160A}	2
*Ba*SatA^{D160E}	2
*Ba*SatA^{D160N}	2
*Ba*SatA^{Y164G}	2
*Ba*SatA^{Y164A}	2
*Ba*SatA^{Y164L}	2
*Ba*SatA^{Y164F}	8
*Ba*SatA^{Y164W}	2

[a]Detailed description of the protocol for MIC determinations is provided in Materials and Methods.

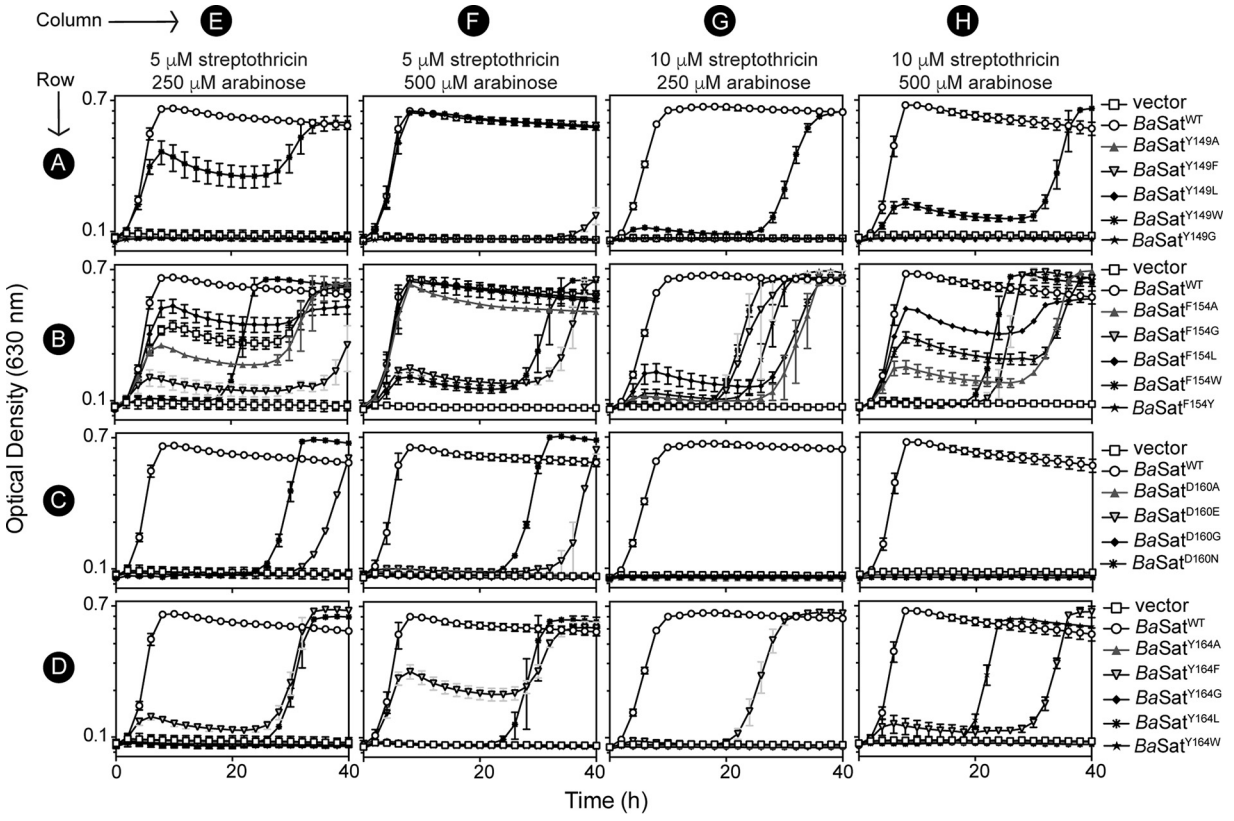

FIG 7 Variant *B. anthracis satA* alleles confer impaired streptothricin resistance to *S. enterica*. Strains carrying wild-type alleles (*B. anthracis satA*$^+$, open circles), variant *B. anthracis satA* alleles, or empty vector (open squares) were grown in glycerol (22 mM) minimal medium and challenged with 5 μM streptothricin (columns E and F) or 10 μM streptothricin (columns G and H) with either 250 μM L-(+)-arabinose (columns E and G) or 500 μM L-(+)-arabinose (columns F and H) for induction. Error bars represent standard deviations. Symbols shown refer to growth curves on that row. All strains carried chromosomal Δ*metE2702 ara-9* mutations and carried the indicated plasmids: JE22263 (/pCV1; squares), JE24022 (/pBaSAT1; circles), JE24312 (/pBaSAT3; triangles), JE24313 (/pBaSAT4; inverted triangles), JE24456 (/pBaSAT12; diamonds), JE24457 (/pBaSAT13; asterisks), JE24586 (/pBaSAT20; stars), JE24314 (/pBaSAT5; triangles), JE24458 (/pBaSAT14; inverted triangles), JE24459 (/pBaSAT15; diamonds), JE24315 (/pBaSAT6; asterisks), JE24460 (/pBaSAT16; stars), JE24461 (/pBaSAT17; triangles), JE24316 (/pBaSAT7; inverted triangles), JE24317 (/pBaSAT8; diamonds), JE24588 (/pBaSAT21; asterisks), JE24318 (/pBaSAT9; triangles), JE24319 (/pBaSAT10; inverted triangles), JE24462 (/pBaSAT18; diamonds), JE24463 (/pBaSAT19; asterisks), and JE24320 (/pBaSAT11; stars). vector, pCV1 (27).

above-mentioned substitutions was assessed *in vivo* in *S. enterica* as before (Fig. 7, row C). Surprisingly, substitutions at D160 resulted in *Ba*SatA variants with greatly reduced or no streptothricin-detoxifying activity (Table 4), with no strain that synthesized a D160 variant able to grow when challenged with 10 μM streptothricin (Fig. 7, row C, columns

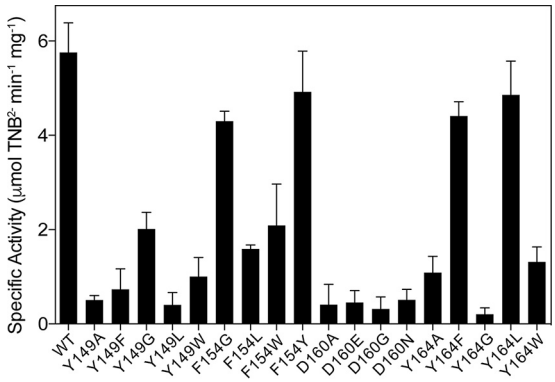

FIG 8 Specific activity of *Ba*SatA and variants. Reaction mixtures of acetyl-CoA, streptothricin, and H_6-*Ba*SatA and variants were incubated at 25°C, and specific activity (μmol TNB^{2-} min^{-1} mg^{-1}) was measured using a continuous spectrophotometric assay as described in Materials and Methods.

G and H). Strains that synthesized variants *Ba*SatA^{D160N} and *Ba*SatA^{D160E} grew in the presence of 5 μM streptothricin after a long growth delay (Fig. 7, row C, columns E and F) but failed to grow when the concentration of streptothricin was doubled to 10 μM, even when the amount of inducer was also doubled (Fig. 7, row C, columns G and H).

The D160 variants were purified and their specific activity measured. Not surprisingly, all D160 variants were only ~10% active relative to the wild-type protein (Fig. 8). In addition, when the variants were tested for their ability to bind streptothricin, none of the D160 variants bound the substrate (Table 2). To determine whether the lack of streptothricin binding of the D160 variants was a direct result of the substituted residues or an indirect effect of protein misfolding, size exclusion chromatography was used to determine whether the D160 variants oligomerized correctly; all D160 variants formed aggregates (Table 1). These data indicated that the perceived lack of streptothricin binding by the D160 variants was due to misfolding of the polypeptide.

DISCUSSION

With the increasing cost of antibiotic resistance, both in terms of monetary and mortality costs, understanding the way in which antibiotic-detoxifying enzymes bind their ligands can aid in the design of inhibitors of such enzymes. Here, we used the streptothricin acetyltransferase SatA from *Bacillus subtilis* and *Bacillus anthracis* as a model to probe for residues important for function and antibiotic binding.

Modeling substitutions into the crystal structure of *Ba*SatA. To better understand how the substitutions analyzed in this work may affect SatA function, we used the reported crystal structure of the *Ba*SatA protein in complex with AcCoA to model the above-mentioned changes. These models are presented in Fig. 9. For clarity, in Fig. 9A *Bs*SatA L128 is equivalent to *Ba*SatA L136, *Bs*SatA A137 is equivalent to *Ba*SatA A145, and *Bs*SatA E129 is equivalent to *Ba*SatA E137.

We speculate that residues L136, E137, and A145 are needed for streptothricin binding and/or correct positioning. The putative role for these residues would be consistent with the severity of their absence for SatA function (Fig. 2, 3, and 6).

Support for this idea was obtained by docking streptothricin into the *Ba*SatA structure (31). In such a model, the amino group of β-lysine is 3.3 Å away from E137, suggesting that this glutamate generates the nucleophile needed to attack the carbonyl group of the acetyl moiety of AcCoA (Fig. 10C, red). It is plausible that in the *Bs*SatA^{L128F} variant (i.e., *Ba*SatA^{L136}) the close proximity of the bulk side chain of phenylalanine to L136 affects the function of the base (Fig. 9A, cyan), abolishing enzyme activity *in vivo* (Fig. 2A and C) and *in vitro* (Fig. 3).

In contrast, the decreased *in vivo* activity of *Bs*SatA^{A137T} does not appear to be a result of hindrance of active-site residues. This idea would be consistent with the location of residue A145, which is found in an α-helix that is more likely to interact with AcCoA (Fig. 9A, cyan). Maurice et al. showed that mutations in the pantothenate binding groove of AAC(6′)-Ib led to changes in substrate specificity (32). Substitutions at residue A137T may cause a conformational change that impairs streptothricin and/or AcCoA binding (Table 2).

Notably, no single-amino-acid variants with substitutions in the putative AcCoA binding pocket were isolated. This may be because multiple residues interact with AcCoA, such as the pyrophosphate binding loop as well as hydrogen bonds of β-sheets with the pantothenic acid moiety (Fig. 9). Hence, a single side chain change would likely be insufficient to block AcCoA from binding SatA.

Some residues are important, but not critical, for SatA function *in vivo*. The two other alleles from our *B. subtilis satA* mutagenesis screen encoded single-amino-acid variants *Bs*SatA^{L126F} (equivalent to *Ba*Sat^{I134F}) and *Bs*SatA^{S84C} (equivalent to *Ba*SatA^{K92C}). Substitutions at these positions yielded enzymes with low levels of activity (Fig. 2B) that detoxified as much streptothricin as the wild-type enzyme when the amount of inducer in the medium was increased (Fig. 2D).

As shown in the *Ba*SatA structure, residues K92 and I134 are located near or at the end of a β-sheet (Fig. 9B, pink). The extent of conformational changes effected by

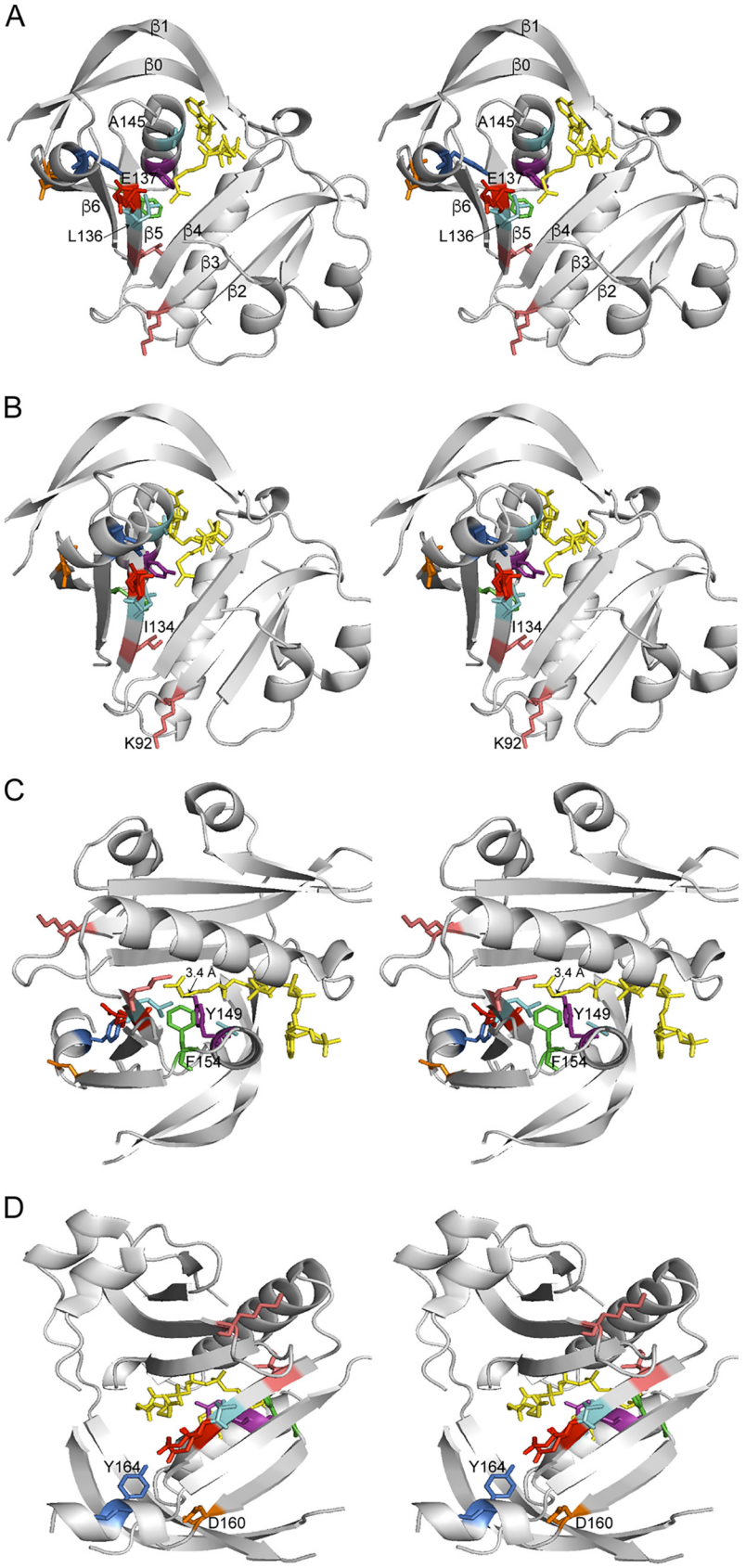

FIG 9 Stereo views of *B. anthracis* SatA structure. Different views of the crystal structure of the SatA from *Bacillus anthracis* strain Ames (PBD entry 3PP9) are shown. Acetyl-CoA is shown in yellow, and residues

(Continued on next page)

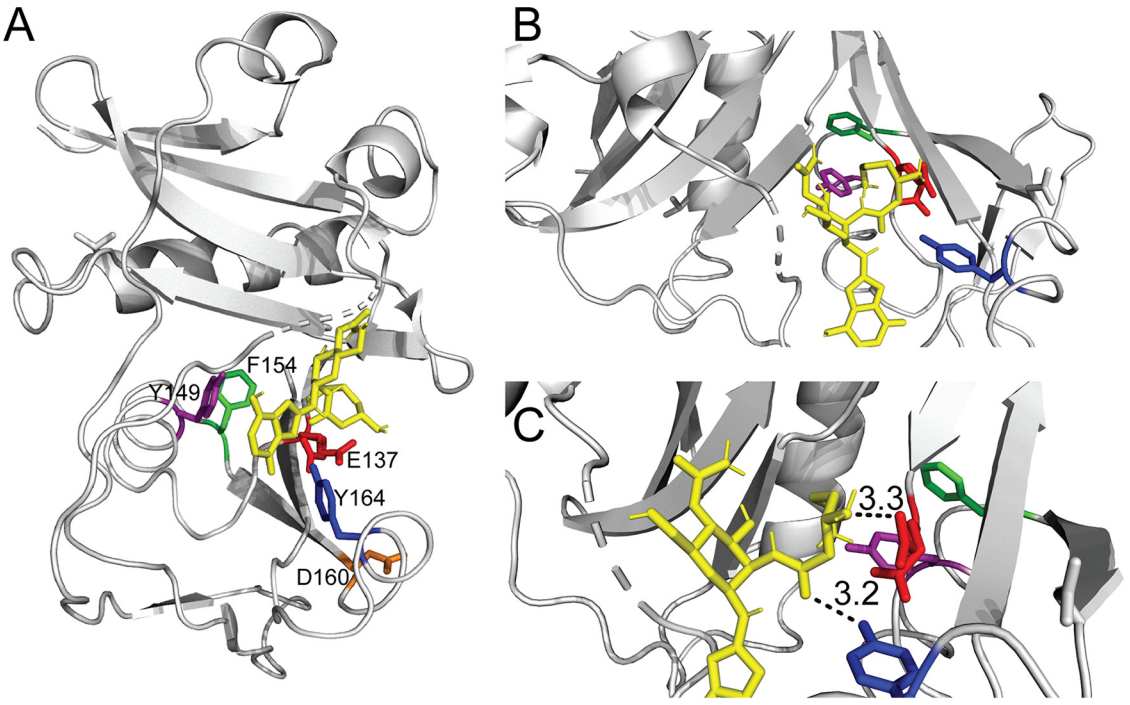

FIG 10 Docking model of streptothricin and *Ba*SatA. AutoDock Vina (31) was used to create a model of streptothricin (shown in yellow) docked to *Ba*SatA. (A) Whole structure of *Ba*SatA highlighting substituted residues. (B) Conserved aromatic residues Y149 (purple), F154 (green), and Y164 (blue) form a pocket around streptothricin, while residue D160 (orange) is found on the dimer interface. (C) Residue E137 (red) is close enough to the beta-lysine for a nucleophilic attack on the amine, suggesting E137 is an active-site acid. Residue Y164 (blue) is in close proximity to interact with streptothricin through hydrogen bonding.

substitutions at positions I134 and K92 is not clear, but we surmised they are not large effects since they did not impact the oligomeric state of the proteins (Table 1). As shown in Fig. 9B, residue I134 is part of β5 and is situated close to the splaying of beta sheets β4 and β5, which is important for AcCoA binding. Thus, substitutions at these positions may disrupt substrate binding, folding, or catalysis.

Conserved aromatic residues are important for *Ba*SatA activity. The crystal structure of *Ba*SatA (20) displays typical GNAT architecture with a core domain comprised of six or seven β-strands and four α-helices (19). The protein binds AcCoA in the V-shaped cleft located between strands β4 and β5 (Fig. 9). Compared to our understanding of AcCoA binding, how GNATs bind their cosubstrate is less known. Recently, Stogios et al. conducted an in-depth study of how the GNAT AAC(6′)-Ig binds aminoglycosides (30). In the structure of the AAC(6′)-Ig/tobramycin complex, nine residues were found to bind the antibiotic. We aligned AAC(6′)-Ig with SatA (see Fig. S4 in the supplemental material) and found that only two of the nine residues were conserved, one of which was the putative active-site base of *Ba*SatA (Fig. S4, green asterisk). This indicates that SatA binds its cosubstrate in a unique way compared to that of AAC enzymes. However, since tobramycin bound the GNAT in a cleft, we focused on

FIG 9 Legend (Continued)
discussed in the text are colored and labeled. (A) The β-sheets are labeled, showing the splaying of β4 and β5 to allow the acetyl-CoA to bind. E137 (red) is predicted to be the active-site glutamate. A change to L136 (cyan) is predicted to interfere with residue E137, while a substitution for residue A145 (cyan) is predicted to disrupt acetyl-CoA binding to SatA. (B) Residues I134 and K92 (salmon) are found at the edges of β-sheets. Substitutions for these residues may impact overall folding of the protein. (C) Residues Y149 (purple) and F154 (green) form a cavity around the acetyl group of acetyl-CoA, forming a putative active-site pocket. The hydroxyl group of Y149 is ~3.4 Å from the sulfur atom of acetyl-CoA and may act as a general acid to reprotonate the thiolate after transfer of the acetyl moiety. (D) Residue Y164 (blue) is parallel to the acetyl group of acetyl-CoA and E137 and is predicted to help position streptothricin for catalysis. Residue D160 (orange) is positioned on the dimer interface and is important for proper dimerization.

conserved SatA residues that appear to form a cleft. In Fig. 9C and D, we highlight three conserved aromatic residues of *Ba*SatA (Y149, purple; F154, green; and Y164, blue) that appear to form a pocket. We hypothesized that these residues are part of the streptothricin-binding pocket. Substitutions for any of these residues negatively affected the ability of *Ba*SatA to detoxify streptothricin (Fig. 7 and Table 4).

Changes to residue Y149 dramatically decreased SatA activity (Fig. 8), even though these variants had binding affinities for streptothricin similar to those of the wild-type enzyme (Table 2). In the model of streptothricin docked to *Ba*SatA (Fig. 10), residue Y149 does not appear to come into direct contact with streptothricin, making it difficult to suggest what its function is. Residue Y149 is ~3.4 Å from the sulfur atom of AcCoA (Fig. 9C) and could act as a general acid that interacts with the thiolate after the acetyl group is transferred, explaining why substitution for this residue led to lowered activity even in the absence of changes to streptothricin binding. There is precedent reported in the literature for tyrosine serving as a general acid for a thiolate anion (33).

Residue F154 also does not appear to interact with streptothricin in the streptothricin-*Ba*SatA model (Fig. 10); however, substitutions at this position did impact antibiotic binding and activity (Table 2 and Fig. 8). Previous studies of GNATs have shown that this position is usually occupied by a phenylalanine or a tyrosine, and substitutions at this position led to enzymes with reduced activity (34–36). For example, mutations to residue F171 of the aminoglycoside 6′-*N*-acetyltransferase [AAC(6′)-Ib] led to an enzyme unable to detoxify kanamycin and amikacin (36). In an alignment of *Ba*SatA with AAC(6′)-Ib, *Ba*SatA F154 corresponds to F171 of AAC(6′)-Ib, suggesting that the two residues play similar roles. Shmara et al. suggested that the phenylalanine or tyrosine in this position helps bind and position AcCoA (34). Upon inspection of the streptothricin-protein model, F154 may be interacting with Y149 via pi stacking (Fig. 10B). The residues are less than 4.5 Å apart, and their relative positions suggest that pi stacking is possible and stabilizes the protein-ligand complex. Previously, mutations disrupting the AcCoA binding of the AAC(6′)-Ib GNAT were shown to increase the antibiotic activity spectrum because of overall structural changes (32). Hence, changes to F154 could result in disruptions of α4, leading to disruptions in cosubstrate binding and activity.

Conserved aromatic residue Y164 is important for streptothricin binding by *Ba*SatA. As suggested by the docking of streptothricin to *Ba*SatA, residue Y164 appears to play a role in streptothricin binding via possible hydrogen bonding (Fig. 10C). This idea is supported by ITC data, in which the *Ba*SatA^{Y164S} variant does not bind streptothricin (Table 2). We did not explore the reason why streptothricin did not bind to this variant. However, we note that the *Ba*SatA^{Y164F} variant, which retains the benzene ring but lacks a hydroxyl, showed streptothricin binding with a K_d approximately thrice that of the wild-type enzyme. Such a decrease in affinity suggests that both the bulk and chemical properties of Y164 are needed to bind streptothricin.

Aspartic acid D160 is necessary for dimerization for *Ba*SatA. Besides the three aromatic residues discussed above, we found a conserved aspartic acid residue (D160) in the hypothesized streptothricin-binding pocket (Fig. 5, orange highlight). Four different substitutions were made at this position, all of which resulted in an almost complete lack of activity (Fig. 7 and 8) and streptothricin binding (Table 2). Importantly, the streptothricin docking model does not indicate a direct interaction of streptothricin and residue D160 (Fig. 10), suggesting a different reason explains the lack of binding. We hypothesized that changes to residue D160 impact folding or dimerization. Either possibility is supported by size exclusion chromatography data, which show that D160 variants formed aggregates instead of dimers (Table 1). The crystal structure of *Ba*SatA places residue D160 close to the dimerization interface (Fig. 9D). The crystal structure shows that C-terminal β-strands come together to form a continuous β-sheet, as shown with other GNATs (33).

Concluding remarks. Taken together, this work revealed residues of the SatA enzyme that are important for streptothricin binding and for proper dimerization. We

TABLE 5 Strains and plasmids used in this study

Strain	Genotype or plasmid[a]	Reference/source[b]
S. enterica JE7088	Δ*metE2702 ara-9*	Strain collection
Derivatives of strain JE7088		
JE22263	/pCV1	26
JE22334	/pBsSATA1	26
JE23884	/pBsSATA10	
JE23657	/pBsSATA4	
JE24032	/pBsSATA9	
JE23887	/pBsSATA11	
JE23888	/pBsSATA12	
JE23889	/pBsSATA13	
JE24022	/pBaSAT1	26
JE24312	/pBaSAT3	
JE24313	/pBaSAT4	
JE24314	/pBaSAT5	
JE24315	/pBaSAT6	
JE24316	/pBaSAT7	
JE24317	/pBaSAT8	
JE24318	/pBaSAT9	
JE24319	/pBaSAT10	
JE24320	/pBaSAT11	
JE24456	/pBaSAT12	
JE24457	/pBaSAT13	
JE24458	/pBaSAT14	
JE24459	/pBaSAT15	
JE24460	/pBaSAT16	
JE24461	/pBaSAT17	
JE24462	/pBaSAT18	
JE24463	/pBaSAT19	
JE24586	/pBaSAT20	
JE24588	/pBaSAT21	
E. coli C41(λDE3)	*ompT hsdS* (r_B^- m_B^-) *gal* (λDE3)	44

[a]A slash indicates that the plasmid was harbored by strain JE7088 (Δ*metE2702 ara-9*).
[b]Unless otherwise stated, strains and plasmids were constructed during the course of this work.

realize the speculative nature of modeling; however, this work has provided testable hypotheses that future work could experimentally address so we can better understand the mechanism of catalysis of the SatA enzyme.

MATERIALS AND METHODS

Culture media and chemicals. Nutrient broth (NB; Difco) supplemented with NaCl (85 mM) was used as rich medium for *S. enterica* strains. Minimal medium for *S. enterica* strains was a no-carbon essential (NCE) minimal medium (37) supplemented with trace minerals, L-methionine (100 μM), and magnesium sulfate (1 mM). For *S. enterica*, 22 mM glycerol was used as the sole carbon and energy source. Ampicillin was used at 100 μg ml^{-1} when necessary (Fisher Scientific). Gold BioTechnology provided HEPES, *tris*(2-carboxyethyl)phosphine hydrochloride (TCEP), isopropyl-β-D-1-thiogalactopyranoside (IPTG), dithiothreitol (DTT), and streptothricin sulfate.

Bacterial strains. *S. enterica* strains are derivatives of *S. enterica* subsp. *enterica* serovar Typhimurium strain LT2 and were constructed during the course of this work (38). All strains and plasmids used are listed in Tables 5 and 6.

Chemical mutagenesis. Variants of *Bs*SatA were obtained using hydroxylamine mutagenesis of a plasmid containing the wild-type allele (pBsSATA1) (26, 39). The high-frequency general transducing bacteriophage P22 HT 105/1 *int-210* was used to infect *S. enterica* cells containing pBsSATA1 (JE22334). The resulting phage lysate was concentrated to ~5.6×10^{11} PFU/ml and was exposed to 0.4 M hydroxylamine in phosphate-EDTA buffer (0.5 M at pH 6; 5 mM EDTA) as described elsewhere (39). This mixture was incubated at 37°C with shaking, and titers of samples of the phage suspension were determined using a P22 phage-sensitive indicator strain every 4 to 8 h until the phage titer was reduced two orders of magnitude (~24 h). To stop mutagenesis, the phage suspension was transferred into 50-ml polycarbonate tubes and pelleted at 20,000 × *g* at 4°C for 2 h using an Avanti J-25I centrifuge equipped with a JA-25.50. The supernatant was decanted, and 1 ml of LSBE (LB with 1 M NaCl and 1 mM EDTA) was added to the phage pellet, which was soaked overnight at 4°C. The resuspended phage was used to transduce the mutagenized plasmid into strain JE7088 (Δ*metE2702 ara-9*), selecting for ampicillin-resistant strains on LB plus ampicillin. After growth at 37°C for ~16 h, ampicillin-resistant colonies were replica printed onto NCE minimal medium plates containing glycerol (22 mM) and ampicillin (100 μg/ml),

TABLE 6 Plasmids used in this study

Plasmid	Allele/description	Encoded variant	Reference[a]
Derivatives of plasmid pCV1[b]			
pBsSATA1	*B. subtilis satA*$^{+}$	*Bs*SatA^{WT}	26
pBsSATA10	*B. subtilis satA2*	*Bs*SatA^{L128F}	
pBsSATA11	*B. subtilis satA3*	*Bs*SatA^{L126F}	
pBsSATA12	*B. subtilis satA4*	*Bs*SatA^{A137T}	
pBsSATA13	*B. subtilis satA5*	*Bs*SatA^{S84C}	
pBsSATA4	*B. subtilis satA6*	*Bs*SatA^{E93Q}	
pBsSATA9	*B. subtilis satA7*	*Bs*SatA^{E129Q}	
pBaSAT1	*B. anthracis satA*$^{+}$	*Ba*SatA^{WT}	26
pBaSAT3	*B. anthracis satA1*	*Ba*SatA^{Y149A}	
pBaSAT4	*B. anthracis satA2*	*Ba*SatA^{Y149F}	
pBaSAT5	*B. anthracis satA3*	*Ba*SatA^{F154A}	
pBaSAT6	*B. anthracis satA4*	*Ba*SatA^{F154W}	
pBaSAT7	*B. anthracis satA5*	*Ba*SatA^{D160E}	
pBaSAT8	*B. anthracis satA6*	*Ba*SatA^{D160G}	
pBaSAT9	*B. anthracis satA7*	*Ba*SatA^{Y164A}	
pBaSAT10	*B. anthracis satA8*	*Ba*SatA^{Y164F}	
pBaSAT11	*B. anthracis satA9*	*Ba*SatA^{Y164W}	
pBaSAT12	*B. anthracis satA10*	*Ba*SatA^{Y149L}	
pBaSAT13	*B. anthracis satA11*	*Ba*SatA^{Y149W}	
pBaSAT14	*B. anthracis satA12*	*Ba*SatA^{F154G}	
pBaSAT15	*B. anthracis satA13*	*Ba*SatA^{F154L}	
pBaSAT16	*B. anthracis satA14*	*Ba*SatA^{F154Y}	
pBaSAT17	*B. anthracis satA15*	*Ba*SatA^{D160A}	
pBaSAT18	*B. anthracis satA16*	*Ba*SatA^{Y164G}	
pBaSAT19	*B. anthracis satA17*	*Ba*SatA^{Y164L}	
pBaSAT20	*B. anthracis satA18*	*Ba*SatA^{Y149G}	
pBaSAT21	*B. anthracis satA19*	*Ba*SatA^{D160N}	
pTEV5	TEV protease-cleavable, N-terminal His_6 tag overexpression vector		45
Derivatives of plasmid pTEV5[c]			
pBaSAT2	*B. anthracis satA*$^{+}$	*Ba*SatA^{WT}	26
pBaSAT22	*B. anthracis satA1*	*Ba*SatA^{Y149A}	
pBaSAT23	*B. anthracis satA2*	*Ba*SatA^{Y149F}	
pBaSAT24	*B. anthracis satA18*	*Ba*SatA^{Y149G}	
pBaSAT25	*B. anthracis satA10*	*Ba*SatA^{Y149L}	
pBaSAT26	*B. anthracis satA11*	*Ba*SatA^{Y149W}	
pBaSAT27	*B. anthracis satA3*	*Ba*SatA^{F154A}	
pBaSAT28	*B. anthracis satA12*	*Ba*SatA^{F154G}	
pBaSAT29	*B. anthracis satA13*	*Ba*SatA^{F154L}	
pBaSAT30	*B. anthracis satA4*	*Ba*SatA^{F154W}	
pBaSAT31	*B. anthracis satA14*	*Ba*SatA^{F154Y}	
pBaSAT32	*B. anthracis satA15*	*Ba*SatA^{D160A}	
pBaSAT33	*B. anthracis satA5*	*Ba*SatA^{D160E}	
pBaSAT34	*B. anthracis satA6*	*Ba*SatA^{D160G}	
pBaSAT35	*B. anthracis satA19*	*Ba*SatA^{D160N}	
pBaSAT36	*B. anthracis satA7*	*Ba*SatA^{Y164A}	
pBaSAT37	*B. anthracis satA8*	*Ba*SatA^{Y164F}	
pBaSAT38	*B. anthracis satA16*	*Ba*SatA^{Y164G}	
pBaSAT39	*B. anthracis satA17*	*Ba*SatA^{Y164L}	
pBaSAT40	*B. anthracis satA9*	*Ba*SatA^{Y164W}	
pTEV16	TEV protease-cleavable, N-terminal His_6 tag overexpression vector		27
Derivatives of plasmid pTEV16[d]			
pBsSATA2	*B. subtilis satA*$^{+}$	*Bs*SatA^{WT}	26
pBsSATA14	*B. subtilis satA2*	*Bs*SatA^{L128F}	
pBsSATA15	*B. subtilis satA3*	*Bs*SatA^{L126F}	
pBsSATA16	*B. subtilis satA4*	*Bs*SatA^{A137T}	
pBsSATA17	*B. subtilis satA5*	*Bs*SatA^{S84C}	

[a]Unless otherwise stated, strains and plasmids were constructed during the course of this work.
[b]The construction of plasmid pCV1 is described in reference 27.
[c]The construction of plasmid pTEV5 is described in reference 45.
[d]The construction of plasmid pTEV16 is described in reference 27.

TABLE 7 Primers used in this study

Primer	Sequence
BaSatA Y149A Forward	GCGTGCAAGTTCGCCGAAAAATGCGG
BaSatA Y149A Reverse	CCGCATTTTTCGGCGAACTTGCACGC
BaSatA Y149F Forward	CGTGCAAGTTCTTCGAAAAATGCGG
BaSatA Y149F Reverse	CCGCATTTTTCGAAGAACTTGCACG
BaSatA Y149G Forward	GCGTGCAAGTTCGGCGAAAAATGCGG
BaSatA Y149G Reverse	CCGCATTTTTCGCCGAACTTGCACGC
BaSatA Y149L Forward	GCGTGCAAGTTCCTCGAAAAATGCGGC
BaSatA Y149L Reverse	GCCGCATTTTTCGAGGAACTTGCACGC
BaSatA Y149W Forward	GCGTGCAAGTTCTGGGAAAAATGCGGC
BaSatA Y149W Reverse	GCCGCATTTTTCCCAGAACTTGCACGC
BaSatA F154A Forward	GAAAAATGCGGCGCTGTGATCGGTGG
BaSatA F154A Reverse	CCACCGATCACAGCGCCGCATTTTTC
BaSatA F154G Forward	GAAAAATGCGGCGGTGTGATCGGTGG
BaSatA F154G Reverse	CCACCGATCACACCGCCGCATTTTTC
BaSatA F154L Forward	GAAAAATGCGGCCTTGTGATCGGTG
BaSatA F154L Reverse	CACCGATCACAAGGCCGCATTTTTC
BaSatA F154W Forward	GAAAAATGCGGCTGGGTGATCGGTGGC
BaSatA F154W Reverse	GCCACCGATCACCCAGCCGCATTTTTC
BaSatA F154Y Forward	CGAAAAATGCGGCTATGTGATCGGTGGC
BaSatA F154Y Reverse	GCCACCGATCACATAGCCGCATTTTTCG
BaSatA D160A Forward	GATCGGTGGCTTCGCATTTCTGGTTTATAAG
BaSatA D160A Reverse	CTTATAAACCAGAAATGCGAAGCCACCGATC
BaSatA D160E Forward	GATCGGTGGCTTCGAATTTCTGGTTTATAAG
BaSatA D160E Reverse	CTTATAAACCAGAAATTCGAAGCCACCGATC
BaSatA D160G Forward	GATCGGTGGCTTCGGATTTCTGGTTTATAAG
BaSatA D160G Reverse	CTTATAAACCAGAAATCCGAAGCCACCGATC
BaSatA D160N Forward	CTTTGTGATCGGTGGCTTCAACTTTCTGGTTTATAAGG
BaSatA D160N Reverse	CCTTATAAACCAGAAAGTTGAAGCCACCGATCACAAAG
BaSatA Y164A Forward	GACTTTCTGGTTGCTAAGGGCCTGAAC
BaSatA Y164A Reverse	GTTCAGGCCCTTAGCAACCAGAAAGTC
BaSatA Y164F Forward	GACTTTCTGGTTTTTAAGGGCCTGAAC
BaSatA Y164F Reverse	GTTCAGGCCCTTAAAAACCAGAAAGTC
BaSatA Y164G Forward	GACTTTCTGGTTGGTAAGGGCCTGAAC
BaSatA Y164G Reverse	GTTCAGGCCCTTACCAACCAGAAAGTC
BaSatA Y164L Forward	CGACTTTCTGGTTCTTAAGGGCCTGAAC
BaSatA Y164L Reverse	GTTCAGGCCCTTAAGAACCAGAAAGTCG
BaSatA Y164W Forward	GACTTTCTGGTTTGGAAGGGCCTGAAC
BaSatA Y164W Reverse	GTTCAGGCCCTTCCAAACCAGAAAGTC
BaSatA Y164S Forward	GACTTTCTGGTTTCCAAGGGCCTGAAC
BaSatA Y164S Reverse	GTTCAGGCCCTTGGAAACCAGAAAGTC
BaSatA Y149S Forward	CGTGCAAGTTCTCCGAAAAATGCGG
BaSatA Y149S Reverse	CCGCATTTTTCGGAGAACTTGCACG
BsSatA E93Q	GTATGCACTAATACAGGACATTGCCG
BsSatA E129Q Forward	CATTTTTGTGGTCTTATGCTTCAGACCCAAGATATTAATATTTC
BsSatA E129Q Reverse	GAAATATTAATATCTTGGGTCTGAAGCATAAGACCACAAAAATG

with or without streptothricin (10 μM); plates were incubated at 37°C for 24 h. Colonies that did not grow on plates with streptothricin were picked from the plate lacking streptothricin, streaked on streptothricin-free plates to free the cells of contaminating phage, and retested for growth on minimal glycerol plates with or without streptothricin (10 μM). Mutagenized plasmids were isolated from strains that still did not grow in the presence of streptothricin, and the *satA* gene in such plasmids was sequenced (Georgia Genomics Facility, University of Georgia, Athens, GA). For plasmids containing a mutation, the *satA* gene was amplified from the mutagenized plasmid and cloned into a fresh vector, which was then sequenced again to verify that only a single mutation was present in the gene. Finally, each reconstructed plasmid carrying a mutant *satA* allele was transformed into a fresh *S. enterica* background. Four *satA* alleles, each containing a single-nucleotide change, were found and further analyzed.

Plasmid construction. All primers used in this study were synthesized by IDT (Coralville, IA) and are listed in Table 7. Mutagenized plasmids served as the template for variant *B. subtilis satA* alleles. The *satA* variant alleles were cloned into both plasmid pCV1 (27), an L-(+)-arabinose-inducible complementation vector, and pTEV16 (27), an IPTG-inducible overproduction vector that added an N-terminal H_6 tag. The *B. anthracis* Ames *satA* (formerly GFG-5714) gene was codon optimized for use in *Escherichia coli* and synthesized by GenScript Biotech Corporation as described previously (26). Site-directed mutants were constructed using the QuikChange protocol (Stratagene) with pBaSat2 used as the template. All vectors were sequenced verified (Georgia Genomics Facility, University of Georgia, Athens, GA).

Growth analyses. *S. enterica* strains were grown at 37°C as described above, and strains were challenged with 5 μM or 10 μM streptothricin. L-(+)-Arabinose inducer was added at a final concentration of 200 μM, 250 μM, or 500 μM.

All growth analyses were performed in 96-well microtiter dishes, with each strain grown under identical conditions in triplicate. Each well contained 198 μl of minimal medium inoculated with 1% (vol/vol) of an overnight starter culture for *S. enterica* strains. All starter cultures were grown for 14 to 16 h on rich medium at 37°C. Cell density was monitored at 630 nm using a computer-controlled ELx808 absorbance plate reader (BioTek Instruments). Readings were acquired every 30 min with continuous shaking. Data were analyzed using the Prism v6 software package (GraphPad Software).

To determine MICs, strains were grown as stated above with various streptothricin concentrations (0 to 50 μM), and MICs were determined after 24 h of growth.

Purification of His_6-tagged variant SatA proteins. N-terminal His_6-tagged *Bs*SatA and *Ba*SatA variants were overproduced in *E. coli* strain C41(λDE3) cells (40) using pTEV16 constructs. Cells were grown and purified as described previously (26). Briefly, cells were grown in 1.5 liters of Terrific broth (Cold Spring Harbor Laboratory Protocols) at 37°C and induced with IPTG (0.5 mM) at an optical density at 600 nm of 0.3 to 0.4. Cultures were grown with shaking overnight at 15°C in a 2.8-liter flask, and cells were harvested by centrifugation at 6,000 $\times$ *g* for 15 min. The cell paste was resuspended in binding buffer containing 4-(2-hydroxyethyl)piperazine-1-ethanesulfonic acid buffer (HEPES; 50 mM, pH 7.5, at 4°C) containing NaCl (500 mM) and imidazole (20 mM), 1 μg ml^{-1} lysozyme, 25 μg ml^{-1} DNase, and 0.5 mM phenylmethanesulfonyl fluoride (PMSF; Fisher Scientific). Cells were broken by sonication, and cellular debris was removed by centrifugation at 40,000 $\times$ *g* for 45 min.

The clarified cell extract was loaded onto 5 ml of nickel-nitrilotriacetic acid affinity resin (HisPur; ThermoFisher Scientific). The column was washed with 10 column volumes of bind buffer (50 mM HEPES, pH 7.5) containing NaCl (500 mM) and imidazole (20 mM), followed by six column volumes of wash buffer (50 mM HEPES, pH 7.5) containing NaCl (500 mM) and imidazole (40 mM). Protein was eluted off the column with six column volumes of elution buffer (50 mM HEPES, pH 7.5) containing NaCl (500 mM) and a high concentration of imidazole (500 mM). Fractions of eluted protein were pooled and dialyzed against HEPES buffer (50 mM, pH 7.5, at 4°C) with decreasing amounts of NaCl down to 150 mM. Purified protein was flash frozen in liquid nitrogen and stored at −80°C until use.

Size exclusion chromatography. Variant H_6-SatA protein (125 to 250 μg) was injected onto a Superose 12 10/300 size exclusion column connected to an ÄKTA pure fast protein liquid chromatography (FPLC) system. The column was equilibrated with HEPES buffer (25 mM, pH 7.5) containing NaCl (150 mM) with a flow rate of 0.5 ml min^{-1}. A mixture of standards (Bio-Rad gel filtration standards; γ-globulin [158 kDa], ovalbumin [44 kDa], myoglobin [17 kDa], and vitamin B_{12} [1.35 kDa]) was applied to the column to generate a calibration curve. Peak analysis was performed using UNICORN v4.11 software (GE Healthcare Life Sciences), and retention times of sample were used to calculate molecular mass.

Determination of kinetic parameters. The kinetic parameters for the *Ba*SatA reaction were determined using a continuous spectrophotometric assay that employed 5,5′-dithiobis-(2-nitrobenzoic acid) (DTNB; Ellman's reagent; Sigma-Aldrich) to measure free thiols of CoA at 412 nm (41–43). Described briefly, reaction mixtures (100 μl) contained HEPES (50 mM, pH 7), DTNB (0.3 mM), SatA (0.5 μg), and various amounts of AcCoA and streptothricin. Reactions were initiated by the addition of AcCoA, and a no-streptothricin control was used to correct for background. When streptothricin was the substrate, AcCoA levels were kept at 500 μM and streptothricin was varied from 500 nM to 50 μM. When AcCoA was the substrate, streptothricin levels were kept constant at saturating levels (25 μM) and acetyl-CoA was varied from 10 μM to 500 μM.

Reaction mixtures were incubated at 25°C, and readings were taken every 5 s over 5 min using a SpectraMax Plus 384 microplate spectrophotometer (Molecular Devices). The molar extinction coefficient used for the concentration of the TNB^{2-} anion was 14,150 M^{-1} cm^{-1} (42). The initial velocity versus the substrate concentration was graphed using Prism v6 (GraphPad) software. Data were fitted into the Michaelis-Menten equation to determine the apparent K_m and V_{max} for *Ba*SatA. Reactions were performed in technical triplicate and biological duplicate, and the averages for both apparent K_m and V_{max} are reported here. Specific activity was measured using the same assay, with AcCoA at 500 μM and streptothricin at 50 μM for *Ba*SatA proteins and 10 μM for *Bs*SatA proteins.

ITC. SatA and SatA variants were dialyzed extensively against HEPES buffer (25 mM, pH 7.5, 150 mM NaCl), and binding assays were performed in a Nano ITC isothermal titration calorimeter (TA Instruments). Streptothricin titrant was solubilized in the final dialysate. Protein was quantified spectrophotometrically (NanoDrop 1000; Thermo Fisher Scientific) using the extinction coefficient (ExPASy) and molecular mass. Protein was present at 15 to 40 μM in the sample cell, and streptothricin (150 to 250 μM) was present in the injection syringe. All samples were degassed for 20 min at 25°C before use. Injections of 2.46 μl every 5 min were performed at 25°C with constant stirring at 350 rpm. ITC data were analyzed using NanoAnalyze software (TA Instruments).

SUPPLEMENTAL MATERIAL

Supplemental material for this article may be found at https://doi.org/10.1128/AEM.03029-18.

SUPPLEMENTAL FILE 1, PDF file, 2.4 MB.

ACKNOWLEDGMENTS

We have no conflicts of interest to declare.

We thank Liju Mathew for assistance with PyMol. We thank William Lanzilotta for assistance with streptothricin docking.

This work was supported by grant R35 GM130399 from the National Institutes of Health to J.C.E.-S.

REFERENCES

1. Thorpe KE, Joski P, Johnston KJ. 2018. Antibiotic-resistant infection treatment costs have doubled since 2002, now exceeding $2 billion annually. Health Aff (Millwood) 37:662–669. https://doi.org/10.1377/hlthaff.2017.1153.
2. Handelsman J, Rondon MR, Brady SF, Clardy J, Goodman RM. 1998. Molecular biological access to the chemistry of unknown soil microbes: a new frontier for natural products. Chem Biol 5:R245–R249.
3. Ananda Baskaran S, Venkitanarayanan K. 2014. Plant-derived antimicrobials reduce E. coli O157:H7 virulence factors critical for colonization in cattle gastrointestinal tract in vitro. Biomed Res Int 2014:212395. https://doi.org/10.1155/2014/212395.
4. Ji Z, Wei S, Zhang J, Wu W, Wang M. 2008. Identification of streptothricin class antibiotics in the early-stage of antibiotics screening by electrospray ionization mass spectrometry. J Antibiot (Tokyo) 61:660–667. https://doi.org/10.1038/ja.2008.93.
5. Haupt I, Hubener R, Thrum H. 1978. Streptothricin F, an inhibitor of protein synthesis with miscoding activity. J Antibiot (Tokyo) 31:1137–1142.
6. Haupt I, Jonak J, Rychlik I, Thrum H. 1980. Action of streptothricin F on ribosomal functions. J Antibiot (Tokyo) 33:636–641.
7. Waksman SA, Woodruff HB. 1942. Streptothricin, a new selective bacteriostatic and bactericidal agent active against gram-negative bacteria. Proc Soc Exp Biol Med 49:207–210. https://doi.org/10.3181/00379727-49-13515.
8. Ji Z, Wang M, Zhang J, Wei S, Wu W. 2007. Two new members of streptothricin class antibiotics from Streptomyces qinlingensis sp. nov. J Antibiot (Tokyo) 60:739–744. https://doi.org/10.1038/ja.2007.96.
9. Zhu CX. 2002. Zhongshengmycin, a new agro-antibiotics. Fine Spec Chem 16:14–17.
10. Kobayashi T, Horinouchi S, Uozumi T, Beppu T. 1987. Purification and biochemical characterization of streptothricin acetyltransferase coded by the cloned streptothricin-resistance gene of *Streptomyces lavendulae*. J Antibiot (Tokyo) 40:1016–1022.
11. Krugel H, Fiedler G, Haupt I, Sarfert E, Simon H. 1988. Analysis of the nourseothricin-resistance gene (*nat*) of *Streptomyces noursei*. Gene 62:209–217.
12. Krugel H, Fiedler G, Smith C, Baumberg S. 1993. Sequence and transcriptional analysis of the nourseothricin acetyltransferase-encoding gene *nat1* from *Streptomyces noursei*. Gene 127:127–131.
13. Fernández-Moreno MA, Vallín C, Malpartida F. 1997. Streptothricin biosynthesis is catalyzed by enzymes related to nonribosomal peptide bond formation. J Bacteriol 179:6929–6936.
14. Okamoto S, Suzuki Y. 1965. Chloramphenicol-, dihydrostreptomycin-, and kanamycin-inactivating enzymes from multiple drug-resistant *Escherichia coli* carrying episome "R." Nature 208:1301–1303.
15. Suzuki Y, Okamoto S. 1967. The enzymatic acetylation of chloramphenicol by the multiple drug-resistant *Escherichia coli* carrying R factor. J Biol Chem 242:4722–4730.
16. Shaw WV, Packman LC, Burleigh BD, Dell A, Morris HR, Hartley BS. 1979. Primary structure of a chloramphenicol acetyltransferase specified by R plasmids. Nature 282:870–872. https://doi.org/10.1038/282870a0.
17. Shaw KJ, Rather PN, Hare RS, Miller GH. 1993. Molecular genetics of aminoglycoside resistance genes and familial relationships of the aminoglycoside-modifying enzymes. Microbiol Rev 57:138–163.
18. Ramirez MS, Tolmasky ME. 2010. Aminoglycoside modifying enzymes. Drug Resist Updat 13:151–171. https://doi.org/10.1016/j.drup.2010.08.003.
19. Vetting MW, de Carvalho LPS, Yu M, Hegde SS, Magnet S, Roderick SL, Blanchard JS. 2005. Structure and functions of the GNAT superfamily of acetyltransferases. Arch Biochem Biophys 433:212–226. https://doi.org/10.1016/j.abb.2004.09.003.
20. Favrot L, Blanchard JS, Vergnolle O. 2016. Bacterial GCN5-related N-acetyltransferases: from resistance to regulation. Biochemistry 55:989–1002. https://doi.org/10.1021/acs.biochem.5b01269.
21. Hegde SS, Javid-Majd F, Blanchard JS. 2001. Overexpression and mechanistic analysis of chromosomally encoded aminoglycoside 2′-N-acetyltransferase (AAC(2′)-Ic) from *Mycobacterium tuberculosis*. J Biol Chem 276:45876–45881. https://doi.org/10.1074/jbc.M108810200.
22. Vetting MW, Hegde SS, Javid-Majd F, Blanchard JS, Roderick SL. 2002. Aminoglycoside 2′-*N*-acetyltransferase from *Mycobacterium tuberculosis* in complex with coenzyme A and aminoglycoside substrates. Nat Struct Biol 9:653–658. https://doi.org/10.1038/nsb830.
23. Draker KA, Wright GD. 2004. Molecular mechanism of the enterococcal aminoglycoside 6′-N-acetyltransferase: role of GNAT-conserved residues in the chemistry of antibiotic inactivation. Biochemistry 43:446–454. https://doi.org/10.1021/bi035667n.
24. Norris AL, Ozen C, Serpersu EH. 2010. Thermodynamics and kinetics of association of antibiotics with the aminoglycoside acetyltransferase (3)-IIIb, a resistance-causing enzyme. Biochemistry 49:4027–4035. https://doi.org/10.1021/bi100155j.
25. Hegde SS, Dam TK, Brewer CF, Blanchard JS. 2002. Thermodynamics of aminoglycoside and acyl-coenzyme A binding to the *Salmonella enterica* AAC(6′)-Iy aminoglycoside N-acetyltransferase. Biochemistry 41:7519–7527.
26. Burckhardt RM, Escalante-Semerena JC. 2017. In *Bacillus subtilis*, the SatA (formerly YyaR) acetyltransferase detoxifies streptothricin via lysine acetylation. Appl Environ Microbiol 83:e01590-17. https://doi.org/10.1128/AEM.01590-17.
27. VanDrisse CM, Escalante-Semerena JC. 2016. New high-cloning-efficiency vectors for complementation studies and recombinant protein overproduction in *Escherichia coli* and *Salmonella enterica*. Plasmid 86:1–6. https://doi.org/10.1016/j.plasmid.2016.05.001.
28. Guzman LM, Belin D, Carson MJ, Beckwith J. 1995. Tight regulation, modulation, and high-level expression by vectors containing the arabinose PBAD promoter. J Bacteriol 177:4121–4130.
29. Hentchel KL, Escalante-Semerena JC. 2015. Acylation of biomolecules in prokaryotes: a widespread strategy for the control of biological function and metabolic stress. Microbiol Mol Biol Rev 79:321–346. https://doi.org/10.1128/MMBR.00020-15.
30. Stogios PJ, Kuhn ML, Evdokimova E, Law M, Courvalin P, Savchenko A. 2017. Structural and biochemical characterization of *Acinetobacter* spp. aminoglycoside acetyltransferases highlights functional and evolutionary variation among antibiotic resistance enzymes. ACS Infect Dis 3:132–143. https://doi.org/10.1021/acsinfecdis.6b00058.
31. Trott O, Olson AJ. 2010. AutoDock Vina: improving the speed and accuracy of docking with a new scoring function, efficient optimization, and multithreading. J Comput Chem 31:455–461. https://doi.org/10.1002/jcc.21334.
32. Maurice F, Broutin I, Podglajen I, Benas P, Collatz E, Dardel F. 2008. Enzyme structural plasticity and the emergence of broad-spectrum antibiotic resistance. EMBO Rep 9:344–349. https://doi.org/10.1038/embor.2008.9.
33. Salah Ud-Din AI, Tikhomirova A, Roujeinikova A. 2016. Structure and functional diversity of GCN5-related N-acetyltransferases (GNAT). IJMS 17:1018. https://doi.org/10.3390/ijms17071018.
34. Shmara A, Weinsetel N, Dery KJ, Chavideh R, Tolmasky ME. 2001. Systematic analysis of a conserved region of the aminoglycoside 6′-N-acetyltransferase type Ib. Antimicrob Agents Chemother 45:3287–3292. https://doi.org/10.1128/AAC.45.12.3287-3292.2001.
35. Panaite DM, Tolmasky ME. 1998. Characterization of mutants of the 6′-N-acetyltransferase encoded by the multiresistance transposon Tn1331: effect of Phen171-to-Leu171 and Tyr80-to-Cys80 substitutions. Plasmid 39:123–133.
36. Chavideh R, Sholly S, Panaite D, Tolmasky ME. 1999. Effects of F171 mutations in the 6′-N-acetyltransferase type Ib [AAC(6′)-Ib] enzyme on

susceptibility to aminoglycosides. Antimicrob Agents Chemother 43:2811–2812.
37. Berkowitz D, Hushon JM, Whitfield HJ, Jr, Roth J, Ames BN. 1968. Procedure for identifying nonsense mutations. J Bacteriol 96:215–220.
38. Ryu J, Hartin RJ. 1990. Quick transformation in *Salmonella typhimurium* LT2. Biotechniques 8:43–45.
39. Davis RW, Botstein D, Roth JR. 1980. A manual for genetic engineering: advanced bacterial genetics. Cold Spring Harbor Laboratory Press, Cold Spring Harbor, NY.
40. Chan CH, Escalante-Semerena JC. 2011. ArsAB, a novel enzyme from *Sporomusa ovata* activates phenolic bases for adenosylcobamide biosynthesis. Mol Microbiol 81:952–967. https://doi.org/10.1111/j.1365-2958.2011.07741.x.
41. Ellman GL, Courtney KD, Andres V, Jr, Featherstone RM. 1961. A new and rapid colorimetric determination of acetylcholinesterase activity. Biochem Pharmacol 7:88–95. https://doi.org/10.1016/0006-2952(61)90145-9.
42. Eyer P, Worek F, Kiderlen D, Sinko G, Stuglin A, Simeon-Rudolf V, Reiner E. 2003. Molar absorption coefficients for the reduced Ellman reagent: reassessment. Anal Biochem 312:224–227.
43. Thao S, Escalante-Semerena JC. 2011. Biochemical and thermodynamic analyses of *Salmonella enterica* Pat, a multidomain, multimeric N(epsilon)-lysine acetyltransferase involved in carbon and energy metabolism. mBio 2:e00216-11. https://doi.org/10.1128/mBio.00216-11.
44. Miroux B, Walker JE. 1996. Over-production of proteins in *Escherichia coli*: mutant hosts that allow synthesis of some membrane proteins and globular proteins at high levels. J Mol Biol 260:289–298. https://doi.org/10.1006/jmbi.1996.0399.
45. Rocco CJ, Dennison KL, Klenchin VA, Rayment I, Escalante-Semerena JC. 2008. Construction and use of new cloning vectors for the rapid isolation of recombinant proteins from *Escherichia coli*. Plasmid 59:231–237. https://doi.org/10.1016/j.plasmid.2008.01.001.